Observation of two charge ordering transitions in the valence-fluctuating EuPtP by resonant x-ray diffraction

T. Inami and S. Michimura
Condensed Matter Science Division, Japan Atomic Energy Agency, Sayo, Hyogo 679-5148, Japan

A. Mitsuda and H. Wada
Department of Physics, Kyushu University, 6-10-1 Hakozaki, Higashi-ku, Fukuoka 812-8581, Japan

(Received 20 May 2010; revised manuscript received 30 October 2010; published 30 November 2010)

Two first-order phase transitions of the valence-fluctuating compound EuPtP at $T_1=246$ K and $T_2=200$ K were examined by means of resonant x-ray diffraction at the Eu L_3 absorption edge. Although previous Mössbauer spectroscopy and preliminary x-ray diffraction experiments have suggested charge-ordered states, characteristic energy spectra of the 111 and $11\frac{2}{3}$ reflections observed in the present experiment unambiguously indicated that twofold and threefold superstructures of Eu valence exist below T_2 and between T_1 and T_2, respectively. We also propose a mechanism to explain the charge ordering in EuPtP based on a charge-lattice coupling that alters a Coulomb repulsion.

DOI: 10.1103/PhysRevB.82.195133 PACS number(s): 61.05.C−, 75.30.Mb, 75.25.Dk

I. INTRODUCTION

Charge ordering is a common phenomenon in condensed-matter physics. Transitions to the charge-ordered state from a uniform intermediate-valence state are observed in a wide range of materials, such as molecular conductors of fractional filling[1,2] and mixed-valence transition-metal oxides,[3,4] as well as valence-fluctuating rare-earth compounds.[5,6] The underlying scenario in these transitions is the competition between the kinetic energy and the intersite Coulomb interactions. For instance, in the magnetite Fe_3O_4, the formal valence of the octahedral site is 2.5+, and hopping of the $3d$ electrons between the Fe^{2+} and Fe^{3+} ions at high temperatures makes these ions crystallographically equivalent. Because of the relatively narrow bandwidth, the intersite Coulomb repulsion overcomes the kinetic energy of the hopping electrons and the charge-disorder entropy at low temperatures, and eventually a static, inhomogeneous valence state is realized below the Verwey transition temperature 123 K.

A charge-ordered ground state is also proposed in the ternary rare-earth compound EuPtP.[7] The above-mentioned, well-established, and very simplified standard model, however, appears to be irrelevant to the charge ordering in EuPtP. The electrical resistivity of EuPtP is metallic,[8,9] and it is considered that the kinetic energy always exceeds the Coulomb repulsion. In fact, EuPtP is categorized in another group of valence-fluctuating materials. In these materials, such as $YbInCu_4$ and $EuPd_2Si_2$, valence transitions (or valence changes) are observed.[10,11] The basic process is thermal activation to other electron configurations from the ground-state configuration in a single rare-earth ion. A typical example is found in the valence change in $EuNi_2P_2$, where the valence of the Eu ions increases from 2.25 (at 300 K) to 2.50 (at 1.4 K) with decreasing temperature.[12] The temperature dependence of the Eu valence $\bar{v}(T)$ is well described by the interconfigurational excitation model, in which the probabilities of the Eu^{2+} and Eu^{3+} configurations P_2 and P_3, respectively, are given by

$$P_2 = \frac{8\exp(-E_{\mathrm{exc}}/kT)}{1+8\exp(-E_{\mathrm{exc}}/kT)} = 1 - P_3 \quad (1)$$

and $\bar{v}(T)$ is obtained from $\bar{v}(T)=2P_2+3P_3$. E_{exc} is the excitation gap between the Eu^{2+} and Eu^{3+} configurations. In short, the ground state and the first excited state are Eu^{3+} with total angular moment $J=0$ and Eu^{2+} with $J=7/2$, respectively, and the Eu valency decreases with increasing temperature, owing to the mixing of thermally excited divalent states. The lattice temperature T is often replaced by an effective temperature $T^*=(T^2+T_f^2)^{1/2}$, where T_f is the so-called valence-fluctuation temperature, which is the measure of hybridization energy of the $4f$ states with conduction-band electrons. There are no hopping $4f$ electrons between Eu^{2+} and Eu^{3+} sites. Excess (or deficient) electrons are freely restored to (or supplied from) the conduction band. This model also reproduces the steep valence change in $EuPd_2Si_2$ very well by incorporating cooperative processes.[11] It also should be noted that the intermediate valence state is not a space average of well-separated divalent and trivalent states but a quantum-mechanical mixture of the $4f^7(Eu^{2+})$ and $4f^65d$ (Eu^{3+}) configurations. The Mössbauer spectra of $EuNi_2P_2$ indicate single absorption lines, that appear between the divalent and trivalent Eu positions, at all temperatures.[12] Hence, a primary question is whether a charge order is truly realized in a system that has no hopping $4f$ electrons. Another question is what a proper mechanism is for stabilizing a charge-ordered state in a system where the total number of f electrons is variable.

EuPtP crystallizes into a hexagonal structure (space group $P6_3/mmc$) and consists of an alternating stack of the Eu and PtP layers along the c axis. The Eu atoms occupy the $2a$ sites [(0,0,0) and (0,0,1/2)] while the atomic positions of the Pt atoms and the P atoms are the $2c$ sites [(1/3,2/3,1/4) and (2/3,1/3,3/4)] and $2d$ sites [(1/3,2/3,3/4) and (2/3,1/3,1/4)], respectively. The unit cell includes two Eu layers and two PtP layers because the platinum position in a PtP layer is substituted by a phosphorus atom in the adjacent PtP layer

and vice versa. The lattice-constant c shrinks a great deal as lowering temperature, particularly at the first-order transitions located at $T_1=235$ K and $T_2=190$ K, while the lattice constant a increases slightly with decreasing temperature.[13] We refer to the phase above T_1, the phase between T_1 and T_2, and the phase below T_2 as the α phase, the β phase, and the γ phase, respectively. A preliminary x-ray diffraction experiment suggests staggered displacement of the PtP layers (and inequivalent Eu environments) along the c axis at low temperatures.[13]

The temperature dependence of the europium valence has already been reported using Mössbauer spectroscopy (MS) and x-ray absorption spectroscopy (XAS).[13] The average valence extracted from XAS measurements increases from 2.16 at 295 K to 2.40 at 4 K while the Mössbauer spectrum directly indicates the inhomogeneous valence state of the Eu ions. At room temperature (α phase), main absorption lines are concentrated at the divalent position. Below T_1 (β phase), the main lines split into large and small absorptions; the larger one is located at the divalent position, whereas the smaller one appears near the trivalent position. Well below T_2 (γ phase), the spectrum consists of two major lines of nearly equal intensities centered at the divalent and trivalent positions. However, the spatial distribution of the two Eu valences is not obtained from MS.

In this study, we carried out resonant x-ray diffraction (RXD) experiments of EuPtP at the Eu L_3 absorption edge. We directly observed spatially ordered valences through the energy spectra of forbidden and superlattice reflections. The outline of this paper is as follows: in the next section, after a general description of RXD is given, details of the experiments are presented. Section III is devoted to showing experimental results and their analysis. A theoretical model is presented in Sec. IV and we discuss a charge-lattice coupling as a possible origin of the charge ordering in metallic EuPtP. A short conclusion is given in Sec. V.

II. EXPERIMENTAL

RXD is a suitable technique for examining a regular array of different electronic states.[5] Near an absorption edge, the atomic scattering factor $f(E)$ is expressed in the form

$$f(E) = f_0 + f'(E) + if''(E), \tag{2}$$

where E is the x-ray energy, f_0 is the normal coherent scattering factor, and f' and f'' are the real and imaginary parts of the dispersion correction. Since the absorption energies are slightly different between the divalent and trivalent states, the dispersion correction of the divalent state (f'_{2+} and f''_{2+}) makes a considerable contrast with that of the trivalent state (f'_{3+} and f''_{3+}) near the absorption edge. Accordingly, if Eu^{2+} and Eu^{3+} layers are stacked in turn along the c axis in EuPtP, for example, the structure factor of the hhl reflection (l =odd integer), which corresponds to the period of this charge ordering, is given by

$$F(hhl) = (f'_{2+} - f'_{3+}) + i(f''_{2+} - f''_{3+}) + F_0, \tag{3}$$

where F_0 is the normal structure factor that comes from the deviation of the atomic positions of the Pt and P atoms from the high-symmetry $P6_3/mmc$ structure. Hence, a characteristic energy dependence is observed in diffraction intensity at "charge-order reflections." Here we assumed that the displacement of the Eu ions is negligible. The validity of this assumption is checked later.

Single crystals of EuPtP were grown from a Pb flux. Powder x-ray diffraction patterns were indexed with a hexagonal structure of $a=4.085$ Å and $c=8.623$ Å. No noticeable extra peak was observed. Magnetic susceptibility was measured with a superconducting quantum interference device magnetometer at a field of 1 T, exhibiting two sharp first-order phase transitions at $T_1=246$ K and $T_2=200$ K in a warming run.[9]

The RXD experiments were performed at BL22XU in SPring-8. X-rays were monochromatized using a Si(111) double-crystal monochromator and the energy width was about 1 eV at 7 keV. A pair of bent and cylindrical mirrors were inserted in order to focus x-rays and reduce higher harmonics. The photon energy was tuned near the L_3 edge of Eu (6.982 keV). The calibration of the photon energy was performed using the K absorption edge of Fe foil. A single-crystalline sample was attached to the cold head of a closed-cycle refrigerator, which was mounted on a four-circle diffractometer with a horizontal scattering plane. The sample was a rectangular parallelepiped of $0.5\times0.3\times0.3$ mm^3 and the largest plane was a (100) plane. We mainly explored the HHL zone. The orientation of the sample was determined using the (100), (110), and (112) reflections. The mosaic width of the (100) reflection of the sample was about 0.01° full width at half maximum at room temperature, indicating the high quality of the crystal.

III. RESULTS AND DISCUSSION

In order to check the consistency between our experiment and previous measurements, we first observed the temperature dependence of the x-ray absorption spectrum between 150 and 275 K with increasing temperature by measuring the fluorescence rate as a function of incident x-ray energy. A scintillation detector was set at the scattering angle (2θ) 90° to reduce background. The self-absorption effect was corrected using a standard method[14] so as to obtain a value of the edge jump consistent with the calculated value.[15] The observed fluorescence intensity was thus converted to the absorption coefficient μ. Three spectra measured at representative temperatures are shown in Fig. 1(a). Two peaks that correspond to divalent and trivalent states are observed in all spectra. At the Eu L_3 edge, x-rays promote a $2p$ electron to an empty $5d$ level, leaving a core hole in the $2p$ orbital. Because of the strong Coulomb interaction between the $4f$ electrons and the core hole, the absorption energy of the divalent state is about 7 eV lower than that of the trivalent state. Owing to the large energy difference between the divalent and trivalent states at the final states, a mixed-valence state in the ground state is completely separated into two eigenstates. Therefore, irrespective of the degree of valence fluctuation, two peaks that correspond to divalent and trivalent states are always observed in x-ray absorption spectra. Hence, if all Eu ions in the sample are equivalent, the va-

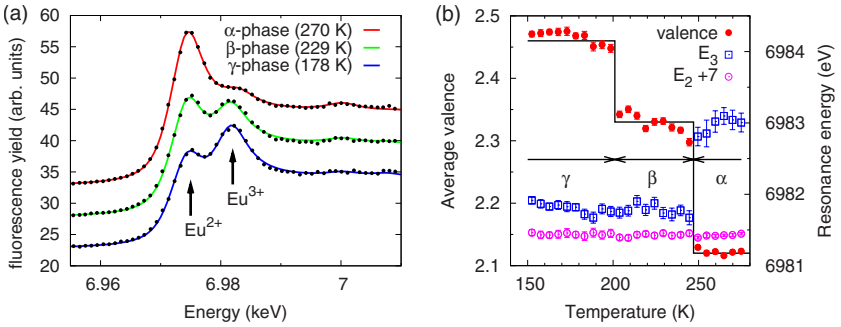

FIG. 1. (Color online) (a) X-ray absorption spectra measured by fluorescence yield at the α phase (top), the β phase (middle), and the γ phase (bottom) and their fits. Absorption correction was made. The spectra are shifted by 5. (b) Average valence of Eu ions and resonance energies of Eu^{2+} state E_2 and Eu^{3+} state E_3 as a function of temperature. E_2 is shifted by 7 eV in order to show in detail the temperature dependence of E_2 and E_3 at high magnification. Solid line is a guide to the eyes.

lency of the Eu ions is obtained from the intensity ratio of the two peaks. In contrast, if there are more than two species of the Eu ions, only the average valence is obtained from XAS.

The corrected absorption spectra (or μ) were fitted with a hyperbolic tangent and two Lorentzians (a white line and a small structure at the high-energy side) for each valence state. We first estimated the line shape of the Eu^{2+} absorption spectrum by fitting data measured in the α phase. Using this function, we then fitted all spectra as the sum of the functions. The relative intensity and the resonance energies of the two peaks were evaluated as fitting parameters. The temperature dependence of the average valence deduced from the relative intensity is shown in Fig. 1(b), as well as the resonance energies of divalent and trivalent states. The average valence exhibits very sharp jumps at T_2=201 K and T_1 =247 K, indicating that remarkable changes in the valence state accompany the first-order transitions. The obtained result substantially agrees with previous XAS measurements,[13] although the transitions are much sharper in our measurement than the reported data. Surprisingly, the resonance energy of the Eu^{3+} also shows clear discontinuity at T_1, whereas no detectable change is observed in the resonance energy of the Eu^{2+} at T_1. This is ascribed to a difference in crystallographic environment around the Eu ions between the uniform valence state (α phase) and the ordered valence state (β and γ phases). The Eu^{3+} final state in the α phase is placed in a nearly divalent circumstance.

RXD measurements were started from a survey on high-symmetry lines (11L, HH1, and 1K0) in order to search for superstructures at 152, 224, and 275 K, and the $(11\frac{1}{3})$ and $(11\frac{2}{3})$ reflections were found at 224 K (β phase). We then measured the peak intensity of the superlattice reflections $(11\frac{1}{3})$, $(11\frac{2}{3})$, $(11\frac{4}{3})$, and $(11\frac{5}{3})$, as well as the forbidden reflection (111), as a function of photon energy at 152, 224, and 275 K. As mentioned in Sec. I, the (111) reflection reflects twofold charge order.

At 152 K (γ phase), the (111) reflection exhibits a characteristic energy dependence, as shown in Fig. 2(b). The (111) reflection is a forbidden reflection under the high-temperature symmetry $P6_3/mmc$ (α phase). Therefore, the substantial intensity observed far from the resonant energy indicates the symmetry breaking of the lattice below $P6_3/mmc$ and agrees with the previous x-ray data.[13]

In contrast, at 224 K (β phase), the intensity of the (111) reflection was very weak. Although contamination of multiple scattering prevents from reaching a firm conclusion, it is likely that the (111) reflection disappears above T_2. Instead, new peaks appeared at the $(11\frac{2}{3})$ and $(11\frac{4}{3})$ positions. The energy dependence of these peaks is similar to that of the (111) reflection at 152 K as shown in Fig. 2(c), whereas the energy dependence measurements revealed that there are no reflections at the $(11\frac{1}{3})$ and $(11\frac{5}{3})$ positions except multiple scattering. Systematic absence of the "odd integer" reflections $(11\frac{l}{3})$, where l=1,3,5,…, crystallographically indicates existence of the c glide plane (or a screw axis), and straightforwardly points out that the period of the charge order is $3c/2$ (or three Eu planes). At 275 K (α phase), no superlattice reflections were observed. Again, existence of the (111) reflection is not conclusive, owing to multiple scattering.

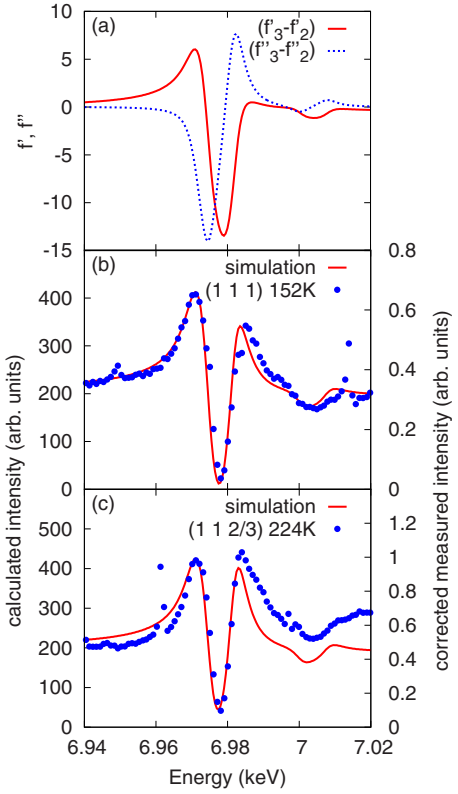

FIG. 2. (Color online) (a) Difference spectra of real part $f'_{3+}-f'_{2+}$ and imaginary part $f''_{3+}-f''_{2+}$ of the dispersion correction. [(b) and (c)] Energy dependence of the peak intensity; (b) the (111) reflection at 152 K (γ phase) and (c) $(11\frac{2}{3})$ reflection at 224 K (β phase). Effect of self-absorption is corrected. Solid lines are fitted curves based on Eq. (3). Small peaklike structures are multiple scattering. Statistical error is smaller than the dot size and the background level is negligible in this figure.

The obtained energy spectra were fitted according to a standard procedure. We assumed that charge-order patterns are $Eu^{2+}Eu^{3+}Eu^{2+}Eu^{3+}$ in the γ phase and $Eu^{2+}Eu^{2+}Eu^{3+}Eu^{2+}Eu^{2+}Eu^{3+}$ in the β phase because (i) the average valance is about 2.47 in the γ phase and 2.33 in the β phase, (ii) the periodicity of the Eu layer is 2 in the γ phase and 3 in the β phase, and (iii) two valence states in the β phase were reported in MS.[13] For these structures, the structure factors of the (111) and $(11\frac{2}{3})$ reflections are equally given by Eq. (3). f'' is obtained from the calculated values and the experimentally observed x-ray absorption constant μ through the relation $f'' \propto \mu E$, where E is the x-ray energy. f' is related to f'' via a Kramers-Kronig transform. We fitted tabulated values[15] of f'' above and below the L_3 edge using a Victoreen function and smoothly connected the fitted curves with f'' of Eu^{2+} extracted from the absorption spectra. We then numerically calculated f' from the fitted values of f''. The obtained f' and f'' were shifted by 7.5 eV and the difference spectra $f'_{3+}-f'_{2+}$ and $f''_{3+}-f''_{2+}$ were obtained as shown in Fig. 2(a). F_0 is a fitting parameter, which was estimated so as to mainly reproduce the amplitude of the oscillatory energy spectra. The results are shown in Figs. 2(b) and 2(c) as solid curves. The calculated curve is in excellent agreement with the measured intensity at 152 K. This is, hence, a direct evidence of the twofold charge ordering along the c axis in EuPtP. In contrast, although agreement between the calculated and measured intensities at 224 K is satisfactory to show the existence of the charge order, it is not yet perfect, probably because of the breakdown of the assumption that the displacement of the Eu ions is negligible in this phase. Both real and imaginary parts of F_0 are required to get a better fit of the energy spectra, indicating the loss of inversion symmetry.

IV. CHARGE-LATTICE COUPLING MODEL

As mentioned in Sec. I, the standard scenario of charge ordering is inappropriate for metallic EuPtP. Hence a new mechanism of charge ordering in EuPtP is required. An important clue is a lattice effect. $EuNi_2(Si_{1-x}Ge_x)_2$ crystallizes in the tetragonal $ThCr_2Si_2$ structure and is a typical valence-fluctuating compound that exhibits valence transitions at around 50–200 K.[16] The Eu valence of the end members of the compounds is, however, temperature-independent 3+ and 2+ for $x=0$ and $x=1$, respectively.[17] In the $ThCr_2Si_2$ structure, the Th atom resides in a space surrounded by eight Si atoms. Hence, a relatively large cage consisting of the Ge atoms matches a large Eu^{2+} ion in $EuNi_2Ge_2$, whereas in $EuNi_2Si_2$ small Eu^{3+} ions are preferable for the small Si framework at all temperatures.

We think that an internal degree of freedom of the lattice stabilizes the charge order in EuPtP. The model is shown in Fig. 3(a), in which a Eu layer is connected to adjacent PtP layers by the force-constant κ. The lattice energy E_p and the interaction between charge and lattice E_{int} are thus given by[18]

$$E_p = \sum_l \frac{\kappa}{2}\{(v_{la+a/2} - u_{la})^2 + (u_{la} - v_{la-a/2})^2\},$$

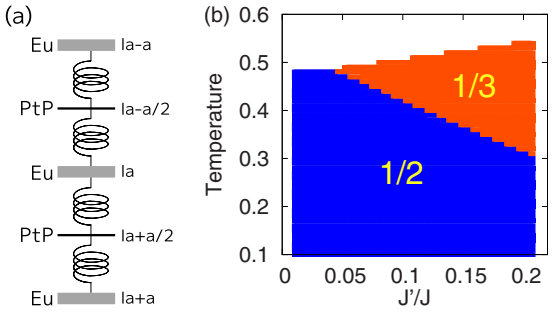

FIG. 3. (Color online) (a) Schematic model of charge-lattice coupling in EuPtP. A Eu layer is connected to adjacent PtP layers through a force constant. (b) Mean-field phase diagram of the extended ANNNI model in external fields with a singlet ground state ($\downarrow$) and octet excited states ($\uparrow$). "1/3" stands for the three-sublattice $\uparrow\uparrow\downarrow$ structure while "1/2" corresponds to the two-sublattice $\uparrow\downarrow$ structure.

$$E_{int} = \sum_l n_{la} g\{(v_{la+a/2} - u_{la}) + (u_{la} - v_{la-a/2})\},$$

where u_{la} and $v_{la+a/2}$ are the displacement of the Eu layer at la and that of the PtP layer at $la+a/2$, respectively, a is the spacing of the Eu layers, and n_{la} equals 1/2 and $-1/2$ for divalent and trivalent layers, respectively. The lattice energy E_p describes Hooke's law, and the interaction term E_{int} represents that divalent and trivalent Eu layers are repulsive and attractive to PtP layers, respectively, when g is negative. For the sake of simplicity, we first enforce the condition $u_{-q}=0$, which corresponds to infinite stiffness between Eu planes. The energy at the equilibrium condition is obtained through $\partial(E_p+E_{int})/\partial v_{-q}=0$, where u_{-q} and v_{-q} are Fourier components of u_{la} and $v_{la+a/2}$. The total-energy E $(=E_p+E_{int})$ is represented as

$$E = -\sum_q \frac{g^2}{\kappa}\sin^2\left(\frac{qa}{2}\right) n_{-q} n_q.$$

By choosing the interacting part and adding the excitation energy E_{exc} for the Eu^{2+} layer, we finally obtain an effective Hamiltonian

$$\mathcal{H} = J\sum_l n_{la} n_{(l+1)a} + E_{exc}\sum_l n_{la}, \tag{4}$$

where $J=g^2/\kappa>0$. This is equivalent to a nearest-neighbor antiferromagnetic (AF) Ising model under magnetic field. It is obvious that the Hamiltonian shows a second-order phase transition to a $\uparrow\downarrow\uparrow\downarrow$ structure for small E_{exc}, where $\uparrow$ and $\downarrow$ denote divalent and trivalent layers.

It is, however, easily found that a next-nearest-neighbor (NNN) AF interaction J' is necessary for stabilizing the $\uparrow\uparrow\downarrow$ structure. By introducing finite stiffness between the Eu planes and between the PtP planes κ_1 and κ_2, respectively, and by relaxing the condition $u_{-q}=0$, the NNN AF interaction $J' n_{la} n_{(l+2)a}$ is naturally derived. The total energy is now given by

$$E = -g^2 \times \sum_q \frac{\kappa + \kappa_1(1-\cos qa)}{\kappa^2 + 2\kappa\kappa_1 + 2\kappa\kappa_2 + 2\kappa_1\kappa_2(1-\cos qa)} n_{-q} n_q.$$

Because of the q-dependent term in the denominator, the interaction becomes long range. If $\kappa < \kappa_1 = \kappa_2$, the ratio J'/J is less than about 0.14. We also phenomenologically incorporated $-\alpha n_{la}^2$ in order to reproduce the experimentally observed first-order nature of the transitions.[11] The Hamiltonian is thus equivalent to an extended axial-NNN Ising (ANNNI) model in external fields.[19] The calculations were carried out up to 20 sublattice using a mean-field approximation in accordance with a standard procedure.[19] Only the singlet ground state and the eightfold first excited state were taken into account. The obtained phase diagram for $J=1$, $E_{\rm exc}=0.05$, and $\alpha=2.5$ is shown in Fig. 3(b). α was chosen so that the valence in the uniform valence state becomes about 2.1 (close to the experimentally observed value). In contrast to the original ANNNI model,[20] in which a nearly infinite number of commensurate phases appear in the phase diagram, only two ordered phases are found in the temperature J'/J space that we surveyed. The two-sublattice "1/2" structure is the ground state and the three-sublattice "1/3" structure presents between the uniform valence state and the "1/2" state at large J'/J. The calculations also show that the uniform valence splits into two valences at a certain temperature when temperature is decreased. Therefore, this model first sets in the three-sublattice $\uparrow\uparrow\downarrow$ charge-ordered state that is followed by the two-sublattice $\uparrow\downarrow\uparrow\downarrow$ structure when J' is large enough, in good agreement with the experiments.

Finally, in Sec. III, we assumed that the valences in the charge-ordered states are integer (Eu^{2+} and Eu^{3+}). Although Mössbauer spectra indicate that valences in the charge-ordered states are very close to Eu^{2+} and Eu^{3+}, there are small deviations in the positions of the absorption lines between the β and γ phases.[13] It is considered that actual valences are $Eu^{2+\delta}$ and $Eu^{3-\delta'}$. However, RXD is based on a virtual x-ray absorption process and, hence, δ and δ' cannot be estimated without knowing a precise value of F_0 in Eq. (3), which is determined in full structural analysis.

V. SUMMARY

We have conducted RXD experiments and confirmed that the successive charge-order phase transitions from a uniform valence state to the staggered two-sublattice $Eu^{2+}Eu^{3+}$ structure with the intervening three-sublattice $Eu^{2+}Eu^{2+}Eu^{3+}$ structure in EuPtP. In order to interpret the charge ordering in metallic EuPtP, we proposed a charge-lattice coupling model and deduced an effective antiferrocoupling between Eu valency. We also found that the observed successive transitions in EuPtP are reduced to a general ANNNI model.

ACKNOWLEDGMENTS

The authors are grateful to O. Sakai for the construction of the theoretical model. This work was partly supported by a Grant-in-Aid for Scientific Research on the Basic Research A (Grant No. 21244056) and that on the Innovative Areas "Heavy Electrons" (Grant No. 21102515) from the Ministry of Education, Culture, Sports, Science and Technology, Japan.

[1] D. S. Chow, F. Zamborszky, B. Alavi, D. J. Tantillo, A. Baur, C. A. Merlic, and S. E. Brown, Phys. Rev. Lett. **85**, 1698 (2000).
[2] T. Kakiuchi, Y. Wakabayashi, H. Sawa, T. Itou, and K. Kanoda, Phys. Rev. Lett. **98**, 066402 (2007).
[3] J. P. Wright, J. P. Attfield, and P. G. Radaelli, Phys. Rev. B **66**, 214422 (2002).
[4] K. Nakamura, T. Arima, A. Nakazawa, Y. Wakabayashi, and Y. Murakami, Phys. Rev. B **60**, 2425 (1999).
[5] U. Staub, B. D. Patterson, C. Schulze-Briese, F. Fauth, M. Shi, L. Soderholm, G. B. M. Vaughan, and A. Ochiai, Europhys. Lett. **53**, 72 (2001).
[6] O. Berkooz, M. Malamud, and S. Shtrikman, Solid State Commun. **6**, 185 (1968).
[7] N. Lossau, H. Kierspel, G. Michels, F. Oster, W. Schlabitz, D. Wohlleben, C. Sauer, and A. Mewis, Z. Phys. B: Condens. Matter **77**, 393 (1989).
[8] A. Nowack, A. Klug, N. Lossau, and A. Mewis, Z. Phys. B: Condens. Matter **77**, 381 (1989).
[9] A. Mitsuda, T. Okuma, K. Sato, K. Suga, Y. Narumi, K. Kindo, and H. Wada, J. Phys.: Condens. Matter **22**, 226003 (2010).
[10] I. Felner, I. Nowik, D. Vaknin, U. Potzel, J. Moser, G. M. Kalvius, G. Wortmann, G. Schmiester, G. Hilscher, E. Gratz, C. Schmitzer, N. Pillmayr, K. G. Prasad, H. de Waard, and H. Pinto, Phys. Rev. B **35**, 6956 (1987).
[11] M. Croft, J. A. Hodges, E. Kemly, A. Krishnan, V. Murgai, and L. C. Gupta, Phys. Rev. Lett. **48**, 826 (1982).
[12] R. Nagarajan, G. K. Shenoy, L. C. Gupta, and E. V. Sampathkumaran, J. Magn. Magn. Mater. **47-48**, 413 (1985).
[13] N. Lossau, H. Kierspel, J. Langen, W. Schlabitz, D. Wohlleben, A. Mewis, and C. Sauer, Z. Phys. B: Condens. Matter **74**, 227 (1989).
[14] S. W. Lovesey and S. P. Collins, *X-Ray Scattering and Absorption by Magnetic Materials* (Clarendon Press, Oxford, 1996), Chap. 5.3.4, pp. 195–197.
[15] Http://lipro.msl.titech.ac.jp/scatfac/scatfac.html
[16] H. Wada, A. Nakamura, A. Mitsuda, M. Shiga, T. Tanaka, H. Mitamura, and T. Goto, J. Phys.: Condens. Matter **9**, 7913 (1997).
[17] G. Wortmann, I. Nowik, B. Perscheid, G. Kaindl, and I. Felner, Phys. Rev. B **43**, 5261 (1991).
[18] O. Sakai, M. Ishii, T. Ogawa, and K. Koshino, J. Phys. Soc. Jpn. **71**, 2052 (2002).
[19] J. Randa, Phys. Rev. B **32**, 413 (1985).
[20] P. Bak and J. von Boehm, Phys. Rev. B **21**, 5297 (1980).